Theory of the [111] magnetization plateau in spin ice

R. Moessner[1] and S. L. Sondhi[2]

[1]*Laboratoire de Physique Théorique de l'Ecole Normale Supérieure, CNRS-UMR8549, Paris, France*
[2]*Department of Physics, Princeton University, Princeton, New Jersey 08544, USA*

The application of a magnetic field along the [111] direction in the spin ice compounds leads to two magnetization plateaux, in the first of which the ground-state entropy is reduced but still remains extensive. We observe that under reasonable assumptions, the remaining degrees of freedom in the low field plateau live on decoupled *kagome* planes, and can be mapped to hard core dimers on a honeycomb lattice. The resulting two-dimensional state is critical, and we have obtained its residual entropy—in good agreement with recent experiments—the equal time spin correlations as well as a theory for the dynamical spin correlations. Small tilts of the field are predicted to lead a vanishing of the entropy and the termination of the critical phase by a Kasteleyn transition characterized by highly anisotropic scaling. We discuss the thermally excited defects that terminate the plateau at either end, among them an exotic string defect which restores three dimensionality.

I. INTRODUCTION

The discovery of the spin ice compounds $Ho_2Ti_2O_7$ (Ref. 1) and $Dy_2Ti_2O_7$ (Ref. 2) is one of the more remarkable events in the study of frustrated magnetism in the last decade. The name spin ice advertises their statistical mechanics at low temperature, which can—approximately—be mapped onto that of an Ising antiferromagnet on the pyrochlore lattice, which in turn is equivalent to cubic ice.[3] The initial discovery stemmed from the observation that the large spins $J_{Ho}=8$ in $Ho_2Ti_2O_7$ failed to order at any temperature despite a ferromagnetic Curie constant.[1] This was understood to result from the interplay of strong easy-axis single-ion anisotropy and the geometry of the pyrochlore lattice, which together effectively turn the ferromagnetic interaction into an antiferromagnetic exchange between Ising pseudospins— which describe whether the moment on a given site is oriented inwards or outwards along the local easy axis passing through the site and the neighboring tetrahedra (see Figs. 1 and 2).[4] Later, it was pointed out that the effective nearest-neighbor ferromagnetic exchange was in large part due to the effect of dipolar interactions projected onto the manifold of Ising states.[5,6]

The antiferromagnetic interaction between the Ising pseudospins generates an "ice rule"—a minimum energy configuration must involve two up and two down pseudospins on each tetrahedron. This ice rule does not, exactly as its cousin the Bernal-Fowler ice rule does not in the case of crystalline water, determine a unique ground state. Rather, there remains a residual extensive zero point entropy, which has been experimentally observed in the case of the Dysprosium ($J_{Dy}=15/2$ with $g\mu_B J_{Dy} \approx 10\mu_B$) spin ice compound in good agreement with calculations and measurements of the entropy of ice.[2] Spin ice therefore offers a laboratory for studying the properties of water ice by proxy, but its properties are, of course, worth studying in their own right. For a review of this burgeoning field, see Ref. 7.

It was realized early on that a magnetic field provides a versatile probe of spin ice, as an external field couples to actual spin magnetic moments and thus acts on the Ising pseudospins in nontrivial ways.[8,9] The phenomena predicted here include plateaux in the magnetization[10,5] and a liquid-gas transition for fields of different strengths and orientations.[10]

Experimentally, the usefulness of magnetic fields was initially limited by the absence of single crystals, so that the behavior in a magnetic field had to be interpreted in terms of an average over all possible relative angles of fields and crystallites. With the advent of single crystals, this shortcoming is being removed.[11–15] In recent experiments on $Dy_2Ti_2O_7$ (Refs. 15, 16) it was demonstrated that applying a field in a [111] direction does indeed lead to the predicted pair of magnetization plateaux—a low field plateau which retains an extensive zero temperature entropy albeit one reduced from the zero field value, and a second plateau at higher fields where the entropy vanishes and the magnetization is saturated upon violation of the ice rule.[5,10]

In this paper we mostly provide a theory of the properties of the low field [111] plateau in the $T \rightarrow 0$ limit with some additional considerations on finite temperature corrections
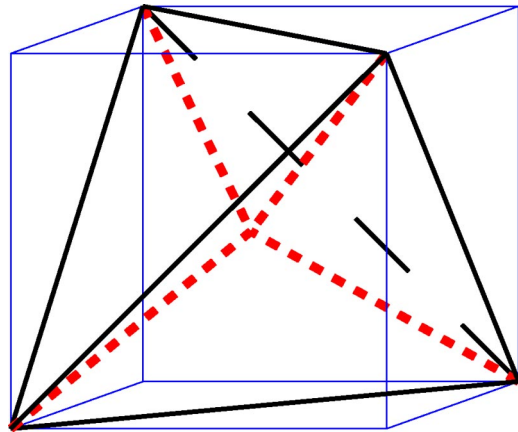

FIG. 1. (Color online) A single tetrahedron inscribed in a cube. In the pyrochlore lattice, the spins reside on the corners of the tetrahedra. In spin ice, they are constrained to point along the body diagonals $\hat{\mathbf{d}}_\kappa$ indicated by the short-dashed lines. The body diagonals define the $\langle 111 \rangle$ directions, the cube edges the $\langle 100 \rangle$ directions, and the bonds the $\langle 110 \rangle$ directions.
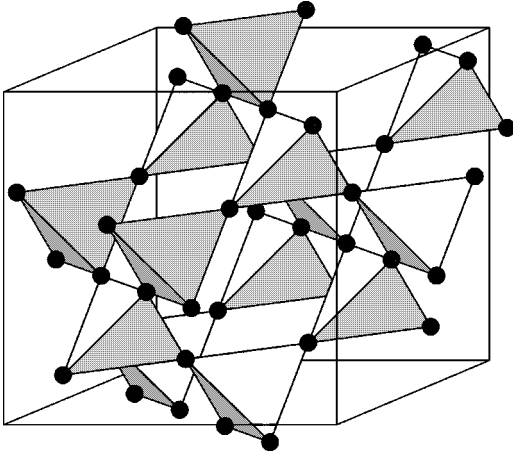
FIG. 2. The pyrochlore lattice. The cube's axes are the same as those in Fig. 1.

and the crossovers out of the plateau at low and high fields. We do so within the nearest-neighbor antiferromagnetic model of spin ice wherein the low-temperature limit serves to enforce the ice rule upon the allowed states. Further, the presence of the magnetic field effects a dimensional reduction in the same limit—the fluctuating degrees of freedom are forced to live on decoupled planar subsets of the parent three dimensional pyrochlore lattice which have the connectivity of the *kagome* lattice. Via a mapping derived previously by us in a study of frustrated Ising models in magnetic fields,[17,18] the remaining planar problem maps onto a hardcore dimer model on the hexagonal lattice. This allows a calculation of the equal time correlations[19]—which are two dimensionally *critical*—and of the (reduced) entropy of this region which agrees well with the experiment. We next consider tilting the field weakly away from the [111] direction, and find that the system remains in an extended critical phase with a continuously drifting wave vector,[19] until it finally undergoes a continuous phase transition, known as the Kasteleyn transition in the dimer literature,[20] where the entropy vanishes. This transition has a number of interesting features, including the absence of any symmetry breaking, a mixed first/second order nature and anisotropic critical exponents. The dimer model has a height representation, and as discussed by Henley,[21] this leads to a natural Langevin dynamics for the coarse grained heights. We use this to write down expressions for the dynamic spin correlations in the plateau, which exhibit a dynamical exponent $z_d = 2$, although testing them is likely to be complicated by equilibration problems that do not affect the thermodynamics and statics. Finally, we identify the excitations out of the ground state manifold, which are a planar zero-dimensional object whose condensation leads to the high field saturated plateau and an unusual infinite string defect, which restores three dimensionality at low fields and analyze their impact on the physics at low temperatures.

In the balance of the paper we will provide details of these assertions. We begin in Sec. II by recapitulating the justification for using the nearest-neighbor model and the ice rule and how they give rise to the plateaux of interest upon addition of a field in the [111] direction. We turn next to the

thermodynamics and statics (Sec. III) and dynamics (Sec. IV) of the plateau. We then discuss the complications produced by the freezing that takes place at low temperatures, in particular with respect to entropy measurements (Sec. V), and then to the impact of thermally excited defects and the longer ranged dipolar physics in Sec. VI. We conclude with a summary.

II. THE MODEL

It is not immediately apparent that the spin ice compounds will exhibit a macroscopic low temperature entropy in zero field, let alone in a field. Indeed, a sufficiently general microscopic model for the spin ice compounds involves exchange couplings, dipolar interactions and a strong easy axis anisotropy. These can be encapsulated in the classical Hamiltonian for unit-length spins $\mathbf{S}_i$:[5,6]

$$\mathcal{H} = \sum_{(ij)} J_{ij} \mathbf{S}_i \cdot \mathbf{S}_j + D \sum_{(ij)} \frac{\mathbf{S}_i \cdot \mathbf{S}_j - 3(\mathbf{S}_i \cdot \hat{\mathbf{r}}_{ij})(\mathbf{S}_j \cdot \hat{\mathbf{r}}_{ij})}{|\mathbf{r}_{ij}|^3}$$

$$+ E \sum_i (\hat{\mathbf{d}}_{\kappa(i)} \cdot \mathbf{S}_i)^2 - g \mu_B J \sum_i \mathbf{B} \cdot \mathbf{S}_i. \quad (2.1)$$

Here J_{ij} are the exchange constants and while the sum on (ij) runs over all pairs of sites, only a few are expected to be significant. The second term is the dipolar interaction of strength D, where $\mathbf{r}_{ij}$ is the vector separation of two spins measured in units of the nearest-neighbor distance, and $\hat{\mathbf{r}}_{ij} = \mathbf{r}_{ij}/|\mathbf{r}_{ij}|$. The third term is the easy axis anisotropy of strength $E < 0$, whose large magnitude is crucial in these compounds and will be taken to infinity for the purposes of this paper, thus constraining the spins to point along their respective easy axes which we have specified by the unit vectors $\hat{\mathbf{d}}_{\kappa(i)}$ at site i. The unit cell of the pyrochlore lattice has four sites, which can be taken to belong to a tetrahedron of one of two orientations, and hence κ runs from 0 to 3 for the four easy axes that point from the center of the tetrahedron to the corner on which the site is located (see Fig. 1). These are the also $\langle 111 \rangle$ directions of the underlying fcc lattice. In the final term, we have allowed for a magnetic field of strength B and $g \mu_B J$ is the magnetic dipole moment of the spins. In the following, we consider fields along (or close to) the [111] direction. This is a threefold symmetry axis of the pyrochlore lattice: a field along the [111] direction singles out the spin ($\kappa = 0$) with an easy [111] axis but leaves intact the symmetry between the other spins (labeled $\kappa = 1,2,3$) with easy axes along the remaining $\langle 111 \rangle$ directions.

The main difficulty in fixing the parameters in Eq. (2.1) is lack of knowledge of the superexchange, while the value of D can be essentially fixed via a crystal field calculation. It turns out that in the spin ice compounds, the effective nearest neighbor exchange is ferromagnetic by virtue of the dipolar interaction, with the weaker superexchange possibly being antiferromagnetic and thereby canceling off part of the dipolar interaction. Very little is known about further-neighbor superexchange, although there again appears to be a cancellation effect against the dipolar interactions.[5,6]

Despite these uncertainties, both experiment and theory indicate that a remarkable simplification takes place at moderate temperatures. If we define the pseudospins $\sigma_i = \pm 1$ by whether a spin points into or out of a tetrahedron on a given sublattice, i.e., we write the spins as $\mathbf{S}_i = \sigma \hat{\mathbf{d}}_{\kappa(i)}$ then the accessible low energy states of Eq. (2.1) in zero field ($\mathbf{B} = \mathbf{0}$) are largely governed by the ice rule, which requires that $|\Sigma_\kappa \sigma_\kappa| = 0$ for each tetrahedron. While Eq. (2.1) is believed to lead to a unique (up to symmetries) ground state at $T = 0$ in zero field,[5,6] this state has in fact not been observed experimentally. Provided Eq. (2.1) is an appropriate description, it thus appears that this state is dynamically inaccessible and irrelevant to the observed physics.[22]

The net result then is that the accessible behavior is captured by the greatly simplified nearest-neighbor Ising pseudospin Hamiltonian

$$\mathcal{H} = J_{\mathrm{eff}} \sum_{\langle ij \rangle} \sigma_i \sigma_j - g\mu_B J \sum_i \mathbf{B} \cdot \hat{\mathbf{d}}_{\kappa(i)} \sigma_i, \qquad (2.2)$$

with an antiferromagnetic J_{eff}.

The ground states of this Hamiltonian for $B = 0$ are, of course, those configurations in which $\Sigma_\kappa \sigma_\kappa = 0$ (i.e., two spins point in and two out) for each tetrahedron separately. The number of these states is not known exactly but an estimate due to Pauling gives $\mathcal{S}_p / k_B = (1/2)\ln(3/2)$ for the ground state entropy per spin which, as mentioned in the Introduction, agrees well with the experimental determination of the residual entropy thus providing support for the simplification.

A. Effect of magnetic field

The effect of switching on a field is strongly dependent on the direction of $\mathbf{B}$, as first discussed in Ref. 10 and is clear from Eq. (2.2). For instance, at zero temperature, an infinitesimal field along the [100] direction completely lifts the degeneracy of the ensemble of spin ice ground states while one in the [110] direction leaves a nonextensive degeneracy.

A field in the [111] direction, which is our subject in this paper, orders one sublattice immediately but still leaves a macroscopically degenerate set of ground states for a finite range of its values, thus producing a magnetization plateau with a residual zero temperature entropy within the ice rule manifold. At a still higher field ($gJ\mu_B B = 6J_{\mathrm{eff}}$) the system abandons the ice rule and chooses the unique configuration that saturates the magnetic moment in the [111] direction and thus exhibits a second magnetization plateau but now with no residual entropy.

To see how this comes about, first note that the projection of the total spin of a tetrahedron onto the magnetic field is maximized in the case of $\sigma \equiv -1$ for $\kappa = 0$ and $\sigma \equiv 1$ for the others. Hence at sufficiently large fields the system will choose the unique configuration in which this arrangement holds for all tetrahedra. This leads, however, to $|\Sigma_\kappa \sigma_\kappa| = 2$ on all tetrahedra and is thus in conflict with the ice constraint $|\Sigma_\kappa \sigma_\kappa| = 0$, so that the low field solution must be different. Instead in that limit one chooses $\sigma_\kappa \equiv 1$ for all the spins on sublattice $\kappa = 0$ as their projection onto the external field is

maximal but as the other spins have an equal projection onto the field, one can choose any one of these to be the second spin with $\sigma = -1$ needed to respect the ice rule. The transition between these two regimes can be located by computing the energies of the two arrangements.

The pyrochlore lattice can be thought of an alternate stacking of *kagome* and triangular planes, with the triangular planes containing all the spins of one of the four spin sublattices—in this case, the triangular planes of the $\kappa = 0$ sublattice are fully polarized and inert. Consequently, the remaining degrees of freedom live on the decoupled *kagome* planes. Each triangle of a given *kagome* plane has two spins with a positive projection ($\sigma = 1$) and one with a negative projection ($\sigma = -1$) onto the external field. Such configurations are equivalent to the ground states of an antiferromagnetic Ising model ($\sigma = \pm 1$) with an exchange in excess of the external field ($\sigma = \{-1, 1, 1\}$ favored over $\sigma = \{-1, -1, 1\}$ in each triangle)[23] and as we show in the next section by explicit enumeration, they are macroscopic in number.

While we have deduced the low field plateau (henceforth simply plateau when no confusion is engendered) and its termination by the saturated state from the nearest-neighbor model, its existence in experiments is further strong evidence for the applicability of the model and can be used to deduce the energy scale for the ice rule.[24]

In the next two sections we will analyze the statics, thermodynamics and dynamics of the plateau at low temperatures within the manifold of *kagome* configurations identified above. In Sec. VI, we will discuss semiquantitatively the consequences of the inclusion of thermally excited defects that either violate the ice rule or are not confined to the *kagome* planes. We also comment briefly there on what might be missed in passing from Eq. (2.1) to (2.2) in our problem. Even with our simplifications we are left with a nontrivial statistical and dynamical problem that needs to be solved in order to compute the physical properties of the plateau and we now turn to this task.

III. PLATEAU: THERMODYNAMICS AND STATICS

In the last section we noted that the allowed spin configurations in a single *kagome* layer in the plateau are equivalent to the ground states of the Ising antiferromagnet on the *kagome* lattice. We have previously considered this problem and shown that the ground states are in correspondence with the configurations of the exactly soluble problem of the dimer model on the honeycomb lattice,[17] a mapping rediscovered by Udagawa *et al.*[18] The triangles of the *kagome* lattice form a dual hexagonal (honeycomb) lattice, whose bonds are the sites of the *kagome* lattice. For each spin with positive projection onto the field, color in the corresponding link of the hexagonal lattice. As each triangle has exactly one such spin, each site of the hexagonal lattice has exactly one colored link emanating from it. By calling the colored link a dimer, one thus establishes an exact one-to-one correspondence between the configurations of a hardcore dimer model on the hexagonal lattice and the spin ice states in a weak [111] field.

```
 141      28       32      105       0        7        60      -16      -10
  -71  24  -52  -104 72  -84  -21   0    0   -90  83  -66   6    2   15   -59  69   -44
   47       155      12      21       90      -17      -8       44      -26
 -113  67 -104  -52  6   -18 -124 103  -90   0    0    17  -84  92  -59   15   7    18
 227      37       46      142      -13       0        67      -32      -22
 -113  31  -68 -170 124 -124  -18  -2   16  -124 124  -84   17   7   25   -68  91   -48
   82       238      0       20      109      -40      -24      44      -42
 -210 128 -170  -68   0    0  -193 173 -124   16   6   35  -104 128  -68   25   18   24
  419       43       68      193      -49      -21      69      -59      -43
 -210  35  -78 -310 242 -193   0    0   49  -170 192 -104   35   24  35   -71  114  -48
  175       388      -49      0       122      -88      -59      35      -66
 -485 310 -310  -78  -13  62  -310 310 -170   49   31  57   -113 172  -71   35   41   25
  970       0        90      248     -140      -80      57     -101      -76
 -485  0    0  -643 552 -310   62   35  105  -210 290 -113   57   67  35   -52  128  -39
  485      643      -242     -97      105     -176     -123      17      -89
-1590 1105 -643   0    0   242  -485 582 -210  105  128   49  -68  192  -52   35   72   17
 3179     -462      0       242     -372     -233      19     -140     -106
-1590 -333 795 -1590 1590 -485  242  310  62   -78  310  -68   49  124   16   -18  124  -21
 1922      795     -1105    -552      18      -242     -173      2      -103
-1111 19189 -1590 795 1105   0    0   552  -78   62  242    0    0   173  -18   16   103   0
 22222    -7599    -1900     0      -475     -304      0      -155     -119
```
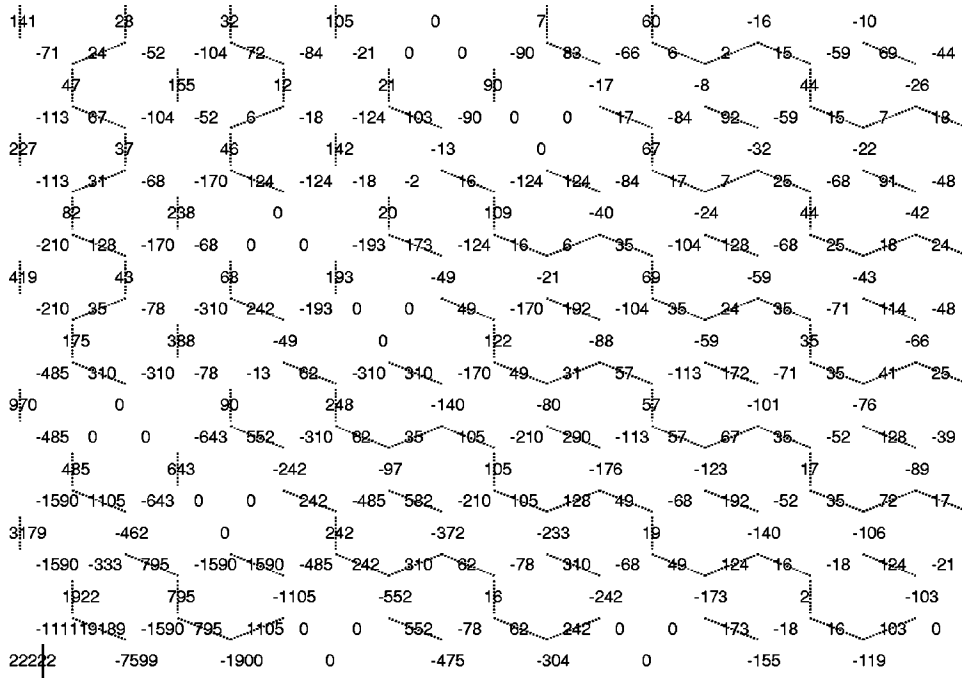
FIG. 3. Short distance correlations $10^5 \times c_{1\kappa}/4$ of the (pseudo)spin in the bottom left hand corner, marked by a solid dimer. Positive correlations are indicated by dashed dimers. This plot uses the same normalization conventions as that of Table I in Ref. 19, hence the factor of 1/4; in the convention of the dimer model, the correlation at the origin is $-1/9 \rightarrow -11111$. Recall that the dimers occupy the links of the hexagonal lattice, the midpoints of which are the *kagome* lattice sites.

A. Entropy

The entropy of the dimer model on the hexagonal lattice is well known, having been first computed as the entropy of the equivalent triangular lattice Ising antiferromagnet at $T = 0$. The latter has an entropy of $\mathcal{S}_\triangle = 0.32306 k_B$ per site. This corresponds to an entropy of $\mathcal{S}_{\text{hexagon}} = \mathcal{S}_\triangle/2$ per site of the dimer model. Each triangle corresponds to a tetrahedron, and hence two sites, of the pyrochlore lattice, so that the entropy per spin equals

$$\mathcal{S} \approx 0.08077 k_B, \tag{3.1}$$

which is, of course, also the value obtained in Ref. 18.

In Ref. 15, the value obtained was $0.096 \pm 0.012 k_B$ per dysprosium atom. While this work was in progress, another measurement has appeared, with a value of $0.078 k_B$.[16] Our value is just outside the error bars of the former. The fact that the former is too high suggests that some configurations breaking the ice rule play a role. Had it been too high, the implication would have been that a certain degree of (possibly short-range) order, presumably due to long range interactions, had already set in. If the latter, however, should turn out to be the correct value in the end, this would be an agreement almost too good to have been hoped for.

By comparison, the zero field result of Ref. 2 is $\mathcal{S}_0 \approx 0.20 k_B$. This compares to the Pauling estimate of $\mathcal{S}_p/k_B = (1/2)\ln(3/2) \approx 0.202733$ or the exact value for two-dimensional spin ice (for which the Pauling estimate is the same) of $\mathcal{S}_{\text{Lieb}}/k_B = (3/4)\ln(4/3) \approx 0.215762$, so that the decrease due to the applied field is by a factor of 2.5–2.7.

B. Correlations

The dimer model describing the plateau has a range of further interesting features in addition to its nonvanishing zero point entropy. Most strikingly, its correlations are critical, decaying as $1/r^2$ at large distances, r.

In detail, consider the connected pseudospin correlation function

$$c_{\kappa\lambda}(\mathbf{r}) = \langle \sigma_\lambda(\mathbf{r})\sigma_\kappa(0)\rangle - \langle\sigma_\lambda\rangle\langle\sigma_\kappa\rangle, \tag{3.2}$$

where $\mathbf{r}$ labels the location of the tetrahedron and the Greek letters the location of a pseudospin in the tetrahedron. This is simply related to the correlation functions of the real spins $C_{\kappa\lambda}(\mathbf{r}) = \langle \mathbf{S}_\lambda(\mathbf{r})\mathbf{S}_\kappa(0)\rangle - \langle\mathbf{S}_\lambda\rangle\langle\mathbf{S}_\kappa\rangle$. For instance, for the components of $\mathbf{S}$ along the [111] direction

$$C_{\kappa\lambda}^{[111]} = (S/3)^2(-3)^{\delta_{\kappa,0}+\delta_{\lambda,0}}c_{\kappa\lambda}, \tag{3.3}$$

where the factors of 3 are due to the different projections of the inequivalent easy axes onto the [111] direction. Similarly, the full spin-spin correlation function is given by

$$C_{\kappa\lambda} = -(S/\sqrt{3})^2(-3)^{\delta_{\kappa,\lambda}}c_{\kappa\lambda}. \tag{3.4}$$

In the plateau region, $\sigma_0 = \langle\sigma_0\rangle = -1$ everywhere, so that $c_{0,\lambda} \equiv 0$. The nontrivial correlations involve only $\kappa > 0$, that is to say spins in the same *kagome* planes. These correlations can be calculated following Ref. 19. We have tabulated the short distance correlations in Fig. 3.

The correlations decay algebraically at long distances. The two independent correlators are
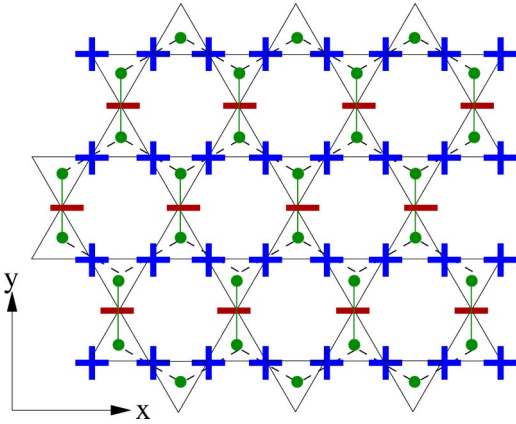
FIG. 4. (Color online) Mapping of pseudospins $\sigma = \pm 1$ on the *kagome* lattice onto hardcore dimers on the (dashed) hexagonal lattice. Shown is the configuration favored by a field tilted slightly away from the [111] direction. The basis vectors used for the *kagome* lattice are also shown.

$$c_{11}(\mathbf{r}) \sim \frac{1}{2\pi^2 r^2}[\cos(4\pi x/3) - \cos(2\theta)],$$

$$c_{12}(\mathbf{r}) \sim \frac{1}{2\pi^2 r^2}[\cos(4\pi x/3 + 4\pi/3) - \cos(2\theta + 4\pi/3)].$$

$$(3.5)$$

Here, $\mathbf{r}$ is a Euclidean coordinate vector for the *kagome* lattice, with $r = |\mathbf{r}|$ being the distance between two triangles of the *kagome* lattice, and $\tan\theta = y/x$, see Fig. 4. This asymptotic behavior, involving a sum of oscillations at wave vector $q_x = 4\pi/3$ and a dipolar piece, can be readily obtained by means of the height representation formulas listed in the next section as well.

As a consequence of the first term in brackets in Eq. (3.6), one would therefore expect a peak in the Fourier transform of the structure factor at wave vector $\pm(4\pi/3, 0)$. Here we have used the lattice constant, twice the pyrochlore nearest neighbor-distance, as the unit of length (see Fig. 4).

The corresponding peaks at the four symmetry related locations are obtained by the appropriate addition of reciprocal lattice vectors $2\pi(1, -1/\sqrt{3})$ and $2\pi(0, 2/\sqrt{3})$. Note in particular that $2\pi(2, 0)$ is the reciprocal lattice vector relating the peaks at $-(4\pi/3)\hat{x}$ and $(8\pi/3)\hat{x}$. However, in Fig. 5, the peak at the latter location is absent. This happens because the "form factor" of the unit cell has a zero at $(8\pi/3)\hat{x}$, as can be verified directly from Eq. (4.4). In Fig. 6, this effect is reversed in that the peak at $(8\pi/3)\hat{x}$ is the stronger one; the peak at $(4\pi/3)\hat{x}$, although present, is not visible on the contour plot for the system size considered as it is almost an order of magnitude weaker.

These are not true Bragg peaks, as there is no long range order. Indeed, as the power law decay of the pseudospin correlations is rather rapid r^{-2} their intensity grows only logarithmically with the planar system size. Similarly, the intensity decreases logarithmically as one moves away from the center of the peak. The second term, although of equal amplitude, does not lead to a feature with macroscopic inten-
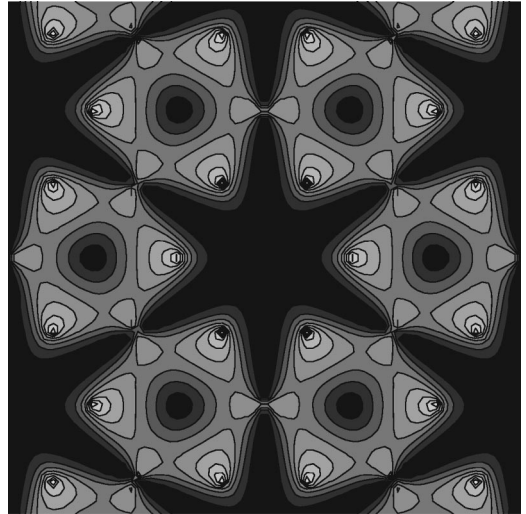

FIG. 5. The Fourier transform of the pseudospin correlations c in the *kagome* planes, obtained from a finite system containing 9604 sites. q_x, q_y range from -4π to 4π. In addition, there is a peak at $q = 0$ and the reciprocal lattice vectors due to the finite average moment induced by the field. Note the logarithmic peak at $(4\pi/3, 0)$ and the symmetry related positions. Together, they should describe the differential cross section found in polarized neutron scattering with the neutron spin pointing along the [111] direction. Light regions denote strong scattering.

sity, as no finite fraction of its weight is concentrated on any one wave vector. In Fig. 5 we plot the absolute value of the Fourier transform of the full pseudospin correlation function, which exhibits these features and is detectable by polarized neutron scattering. In Fig. 6 we plot the cross section for unpolarized neutrons; the difference in the two figures reflects the nontrivial relation between the spins and the pseudospins. Both figures omit the magnetic Bragg peaks that will arise from the static magnetization produced by the applied field, and are obtained for zero out-of-plane wave vector transfer.
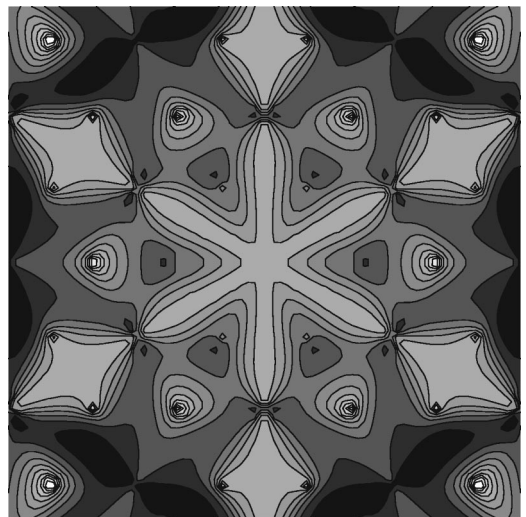

FIG. 6. The Fourier transform of the correlation of the spins components perpendicular to the in-plane wave vector. Details as in the previous figure. The quantity plotted here is also the differential neutron scattering cross section for unpolarized neutrons.

C. Kasteleyn transition in a tilted field

A broader view of the critical correlations in the honeycomb dimer model is obtained by generalizing it to allow for unequal fugacities for dimers of different orientations. As shown by Kasteleyn,[20] the equal fugacity point sits in a critical phase which borders a "frozen" phase with vanishing entropy that is reached by an unusual transition that bears his name. If z_1, z_2, and z_3 are the fugacities of the three sets of dimers, the transition takes place when the fugacity of one set equals the sum of the other two, say $z_1 = z_2 + z_3$. For $z_1 > z_2 + z_3$ a unique configuration survives (shown in Fig. 4). It is interesting to ask whether this phase transition can be realized in the spin ice problem. It turns out that this can be done rather simply by tilting the field.

To see this consider tilting the applied field away from the [111] direction so that it acquires an enhanced component in the [-1-11] direction, which is the easy axis of sublattice $\kappa = 1$: $\mathbf{B} = B(\cos \phi [111]/\sqrt{3} + \sin \phi [\text{-1-12}]/\sqrt{6})$, so that the angle the field makes with the [111] direction is given by ϕ. This keeps the other two of the three *kagome* spin sublattices ($\kappa = 2,3$) equivalent and singles out the $\kappa = 1$ sublattice. To leading order in the tilt angle, spins on sublattice $\kappa = 0$ do not experience a change in energy, whereas spins on the other sublattices do:

$$E_0^B = g \mu_B B J \sigma_0 \cos \phi,$$

$$E_1^B = -(g \mu_B B J/3) \sigma_1 [\cos \phi - 2\sqrt{2} \sin \phi],$$

$$E_{2,3}^B = -(g \mu_B B J/3) \sigma_{2,3} [\cos \phi + \sqrt{2} \sin \phi]. \quad (3.6)$$

As the dimer fugacities are $z_\kappa = \exp[2E_\kappa^B/(k_B T)]$, it follows that the effect of the tilted field is to make them unequal—specifically, to privilege the occupation of vertical dimers over the other two orientations in Fig. 4. At zero temperature z_1 is infinitely bigger than z_2 or z_3 at any tilt angle and the system is deep in the frozen phase, which is to say the energy gain is all there is and we obtain just the so-called staggered configuration shown in Fig. 4.

At nonzero temperatures, or finite fugacities, however, the gain in energy must compete with the loss of entropy, both extensive, to effect a gain in free energy and we obtain a finite range of stability for the critical phase terminated by the Kasteleyn transition. From the criterion $z_1 = z_2 + z_3$ we can deduce a critical tilt angle ϕ_c, set by $k_B T = (2\sqrt{2}/\ln 2) g \mu_B B J \sin \phi$, at which the transition occurs. Note that the transition temperature is proportional to the in-plane field strength $B \sin \phi$, so that the experiment can, in principle, be done at $T \ll B$ and when the tilt angle is sufficiently small to justify our neglect of $O(\phi^2)$ terms. In the following, we express the dependence on the various parameters via $z = z_2/z_1$.

Various predictions follow from this analysis.

(a) The Kasteleyn transition involves a critical vanishing of the entropy

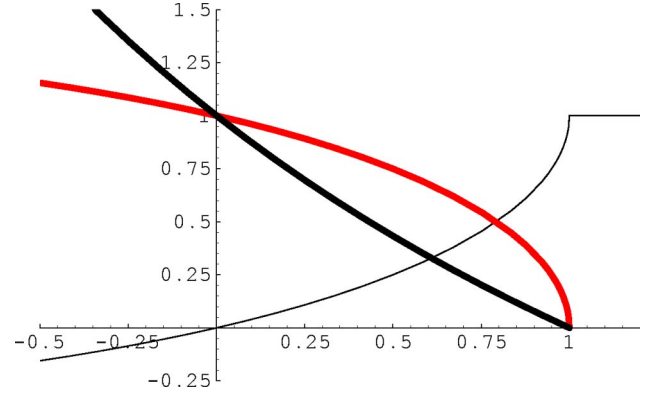$$\mathcal{S} \sim (\phi_c - \phi)^{1/2} \quad (3.7)$$

FIG. 7. (Color online) Magnetization of the spins in the *kagome* planes in the [-1-12] direction (thin line) and inverse correlation lengths (thick lines) in the x direction and y direction (in black). The former is normalized with respect to the saturation magnetization for $B > B_c$, $m_{\text{sat}} = (4\sqrt{2}/3) g \mu_B J$. Saturation for $B \to -\infty$ is half this value (and negative). The inverse correlation lengths are normalized to their zero field value of $2\pi/3$. Note that they vanish with different powers at the transition. The x coordinate is given by $(2\sqrt{2}/\ln 2) g \mu_B B J \sin \phi/(k_B T)$, so that the critical point is located at 1.

that can be detected via standard thermodynamic measurements. In equilibrium this implies a significant signature in the tilt specific heat C in the form of a divergence

$$C \sim \frac{\partial \mathcal{S}}{\partial \phi} \sim (\phi_c - \phi)^{-1/2} \quad (3.8)$$

but freezing is likely to complicate such a direct measurement as we discuss in Sec. V.

(b) The expectation values of the Ising spins for $z > 1/2$ is given by

$$\langle \sigma_1 \rangle = -1 + \frac{4}{\pi} \arcsin \left[\sqrt{1 - \frac{1}{4z^2}} \right],$$

$$\langle \sigma_2 \rangle = \langle \sigma_3 \rangle = (1 - \langle \sigma_1 \rangle)/2. \quad (3.9)$$

The magnetization in the [-1-12] direction, $m_\perp$, being proportional to $\langle \sigma_1 \rangle$, it follows that it deviates in the critical region from its saturation value $m_\perp^{\text{sat}}$ as

$$m_\perp - m_\perp^{\text{sat}} \sim (\phi_c - \phi)^{1/2}. \quad (3.10)$$

This expression holds to the left of the critical point ($z \geq 1/2$, see Fig. 7). To the right, there are no fluctuations, and $\langle \sigma_2 \rangle = \langle \sigma_3 \rangle = -\langle \sigma_1 \rangle = 1$.

The correlations remain critical but change continuously as B is tilted. For example, the equation for the same sublattice connected correlations, Eq. (3.5), is generalized to[19,25]

$$c_{11}(\mathbf{r}') = \frac{1}{2\pi^2 r'^2} [\cos(2x/\xi_x) - \cos(2\theta')]. \quad (3.11)$$

Here $r'^2 = x^2 + (\xi_x/\xi_y)^2 y^2$, with

$$1/\xi_x = 2 \arcsin \sqrt{1 - 1/4z^2}, \quad (3.12)$$

$$1/\xi_y = (4z/\sqrt{3})\sqrt{1-1/4z^2}\arcsin\sqrt{1-1/4z^2},$$

with $z = z_2/z_1 = \exp[2(E_2^B - E_1^B)/(k_B T)]$ and $\tan\theta' = (x/\xi_x)/(y/\xi_y)$. From this we observe the following.

(c) The location of the peak in the structure factor, which remains logarithmic, is given by $\pm(2/\xi_x, 0)$, so that it drifts continuously from $(4\pi/3)\hat{x}$ to the center of the Brillouin zone, which it reaches at the phase transition. Observation of this drift with field tilt should be a good flag of the unusual critical phase.

(d) The scattering pattern is reduced in symmetry—the applied field reduces the sixfold rotational symmetry of the lattice to a twofold one. In particular, this leads to anisotropic scaling at the Kasteleyn transition in which there are two diverging correlations lengths along $[\xi_x \sim (\phi - {}_c\phi)^{-1/2}]$ and transverse $[\xi_y \sim (\phi_c - \phi)^{-1}]$ to the in-plane field, whose ratio ξ_y/ξ_x also diverges as one approaches the transition $z \to 1/2^+$.

(e) Finally we note that the transition is asymmetric. On the side $z \to 1/2^-$, no fluctuations are present, so that the transition has an asymmetric first/second order appearance. However, the latter property is strictly dependent on the hardcore condition on the dimers and tetrahedra violating the ice rule will allow some fluctuations even beyond the transition, see Sec. VI.

IV. PLATEAU: DYNAMICS

We now turn to the dynamical correlations in the plateau continuing to assume that the system explores only its ground state manifold; we will return to the validity of this approximation in Sec. V. *Prima facie*, finding the time dependent correlations seems a difficult task since the configurations are characterized by a local constraint, which we have compactly represented by the hard core dimer mapping. Nevertheless, this can be done at long wavelengths and low frequencies, following the ideas of Henley on the dynamical correlations of critical dimer models,[21] which we apply to the honeycomb lattice in the following. Henley's basic insight is that the dimer configurations on bipartite lattices have a height representation whose fluctuations are *unconstrained* at long wavelengths. For the statics this has been known since the work of Ref. 26 (see also Refs. 21 and 27 for a concise introduction) and the extension to dynamics leads naturally to a Langevin dynamics for the heights. The resulting theory is Gaussian and exhibits dynamic scaling with the dynamic exponent $z_d = 2$. We now give brief details of this analysis.

First, we provide a description of the relevant height model. Microscopically, this involves a map between dimer configurations and the configurations of a surface specified by giving its local height above the dimer plane. The microscopic heights are a set of integers, defined on the sites of the triangular lattice dual to the hexagonal lattice the dimers reside on. The height changes by $+2$ (-2) if one crosses a dimer when going from one site to its nearest clockwise neighbor on an up (down) triangle. If no dimer is crossed, the change is -1 ($+1$). This provides a mapping of dimers onto heights. The dimer density n_d is thus given by $n_d = (\nabla^{\text{lat}}h + 1)/3$, where ∇^{lat} denotes the lattice derivative correspond-

ing to the rules defined in this paragraph.

In the coarse grained, continuum theory, this microscopic expression indicates the identification

$$n_d = \frac{1}{3}(\hat{e}\cdot\nabla)h + \frac{1}{3}, \tag{4.1}$$

where $\hat{e}$ is a unit vector perpendicular to the orientation of the dimer. This is, however, not the full expression, even at leading order. Upon coarse graining, a second nontrivial term appears in the expression for n_d, which reflects the important fluctuations near the characteristic wave vector of the flat states—this is the analog of the staggered "$2k_f$" piece that appears in the bosonization of one-dimensional quantum fermion systems. This piece can be identified by noting that the mapping of dimers onto heights is one-to-many: a shift of the height by 3 units returns the same dimer configuration, and thus the operator must be invariant under this operation.[26] One thus obtains for the dimer densities n_κ:

$$n_1 - \frac{1}{3} = \frac{1}{3}\partial_x h + \zeta[\exp(2\pi ih/3)$$
$$\times \exp(4\pi ix/3) + \text{c.c.}],$$

$$n_2 - \frac{1}{3} = \frac{1}{3}\left(-\frac{1}{2}\partial_x + \frac{\sqrt{3}}{2}\partial_y\right)h + \zeta[\exp(2\pi ih/3)$$
$$\times \exp(4\pi ix/3 + 4\pi i/3) + \text{c.c.}],$$

$$n_3 - \frac{1}{3} = \frac{1}{3}\left(-\frac{1}{2}\partial_x - \frac{\sqrt{3}}{2}\partial_y\right)h + \zeta[\exp(2\pi ih/3)$$
$$\times \exp(4\pi ix/3 - 4\pi i/3) + \text{c.c.}], \tag{4.2}$$

where the normalization $\zeta = 1/(2\pi a)$ involves a short distance cutoff a. There are, of course, corrections from less relevant operators which we have not considered here.

To calculate the static dimer correlators, one uses the fact that the heights fluctuate in a Gaussian manner in equilibrium

$$H = \int d^2r \frac{K}{2}|\nabla h|^2 \tag{4.3}$$

($K = \pi/9$ for the honeycomb lattice), whence the height correlator is given as $\langle h(r)h(0)\rangle = -\ln(r/a)/(2\pi K)$. From these we find the asymptotic correlations

$$c_{ij}(\mathbf{r}) = \frac{1}{2\pi^2 r^2}\{\cos[4\pi x/3 + 4\pi(j-i)/3]$$
$$- \cos[2\theta + 4\pi(i+j-2)/3]\}, \tag{4.4}$$

in agreement with Eqs. (3.6). One sees that the two pieces in the dimer correlators arise from the "uniform" and "staggered" pieces of the representations given above. It is also straightforward to check that the structure factor, at this level of approximation, gets no contribution from the uniform pieces and consists entirely of the logarithmic peaks at

$\pm 4\pi/3\hat{x}$ and related points. In addition, the extinction of the peaks at $\pm 8\pi/3\hat{x}$ in Fig. 5 also follows from Eq. (4.4).

To obtain the dynamical correlations, we note that the long wavelength, low frequency dynamics for a generic local dimer dynamics will be governed by Henley's Langevin equation[21]

$$\frac{dh(\mathbf{r})}{dt} = -\Gamma\frac{\delta H}{\delta h(\mathbf{r})} + \zeta(\mathbf{r},t), \qquad (4.5)$$

where Γ is a kinetic coefficient set by microscopics and the noise $\zeta(\mathbf{r},t)$ obeys

$$\langle \zeta(\mathbf{r},t)\zeta(\mathbf{r}',t')\rangle = 2\Gamma\delta(\mathbf{r}-\mathbf{r}')\delta(t-t'). \qquad (4.6)$$

As this is again a Gaussian theory, it follows that the only non-trivial correlator of the heights is the two-point function

$$\langle \tilde{h}_q(t)\tilde{h}_{-q}(0)\rangle = \frac{1}{Kq^2}\exp[-\lambda(q)t], \qquad (4.7)$$

where $\tilde{h}_q(t)$ is the height configuration at wave vector $q = (q_x, q_y)$ and time t. The relaxation rate for the modes with wave vectors of magnitude q is given by $\lambda(q) = \Gamma K q^2$, which implies a critical dynamics with $z_d = 2$.

The dynamic correlations can now be obtained from this expression in the same manner as the static one. For example, the uniform piece of the same sublattice correlator equals

$$\langle \tilde{n}_{1_q}(t)\tilde{n}_{1_{-q}}(0)\rangle_u = \frac{q_x^2}{Kq^2}\exp[-\lambda(q)t], \qquad (4.8)$$

which yields the further Fourier transform

$$\langle \tilde{n}_{1_{q,\omega}}\tilde{n}_{1_{-q,-\omega}}\rangle_u = \frac{q_x^2}{Kq^2}\frac{q^2}{q^4+w^2}. \qquad (4.9)$$

As in the case of static correlations, the structure factor gets no contribution from such uniform pieces.

The nonzero contribution then comes from the staggered piece which is first calculated in real space as the vertex operator correlator

$$\langle n_1(r,t)n_1(0,0)\rangle_s = \zeta^2\{e^{4\pi ix/3}\langle e^{2\pi ih(\mathbf{r})/3}e^{-2\pi ih(0)/3}\rangle + \text{c.c.}\}$$

$$= 2\zeta^2\cos\left(\frac{4\pi x}{3}\right)\exp\left(-\frac{4\pi^2}{9}C(r,t)\right),$$

where

$$C(r,t) = \langle[h(r,t)-h(0,0)]^2\rangle/2$$

$$= \int\int\frac{d^2q}{(2\pi)^2}\frac{1}{Kq^2}[1-\exp(-\Gamma Kq^2t)\cos(\mathbf{q}\cdot\mathbf{r})].$$

$$(4.10)$$

In the scaling limit $(r,t)\to\infty$ with r^2/t fixed this can be written in the scaling form

$$\langle n_1(r,t)n_1(0,0)\rangle_s = \frac{1}{2\pi^2r^2}\cos\left(\frac{4\pi x}{3}\right)g\left(\frac{r^2}{\Gamma Kt}\right), \quad (4.11)$$

where the scaling function is given in terms of the incomplete Gamma function as

$$g(x) = e^{-\Gamma(0,x/4)} \qquad (4.12)$$

and exhibits the asymptotics

$$g(x) \sim \begin{cases} e^{\gamma}x/4, & x\ll 1, \\ 4\exp(-x/4)/x, & x\gg 1. \end{cases} \qquad (4.13)$$

The former encodes the autocorrelation

$$\langle n_1(0,t)n_1(0,0)\rangle_s = \frac{e^{\gamma}}{8\pi^2}\frac{1}{\Gamma Kt}, \qquad (4.14)$$

where $\gamma = 0.5772\cdots$ is the Euler-Mascheroni constant.

The remaining task is to obtain the Fourier transform of Eq. (4.11) which does not appear possible in closed form and will therefore probably have to be accomplished numerically if desired. However, the essential features can be deduced as follows.

First, the Fourier transform will still be peaked about $\pm(4\pi/3)\hat{x}$ and symmetry related points. Second, if we measure momenta from each of these values, the result exhibits the scaling form

$$\langle \tilde{n}_{1_{q,\omega}}\tilde{n}_{1_{-q,-\omega}}\rangle_s = \frac{1}{|\omega|}\tilde{g}\left(\frac{\Gamma Kq^2}{|\omega|}\right). \qquad (4.15)$$

Third, one can show that

$$\tilde{g}(x) \sim \begin{cases} 1/2, & x\ll 1, \\ c/x, & x\gg 1 \end{cases} \qquad (4.16)$$

with some constant c and that the corrections about either limit are analytic. Together, the last two features imply that fixed frequency cuts will exhibit peaks of height $(2|\omega|)^{-1}$, finite with divergent system size, whose widths will exhibit the characteristic $z_d = 2$ scaling $\Delta q \sim \sqrt{\omega/\Gamma K}$. The complementary fixed q cuts will exhibit a diffusive peak at $\omega = 0$ of height $c/(\Gamma Kq^2)$ and width $\Delta\omega \sim \Gamma Kq^2$.

It is worth noting that in taking the scaling limit we have kept all information relevant to long wavelengths and low frequencies but if we attempt to reconstruct the equal time correlator we will find a spurious ultraviolet singularity. Likewise the large frequency behavior at a fixed q will be softer than the $1/|\omega|$ dependence implied by the scaling form.

V. FREEZING

This is a good place to note an important subtlety in making contact between our analysis, and indeed all theoretical work on ice and spin ice, and the experimental systems. This is the feature that both ice and spin ice exhibit diverging relaxation times (set by the temperature dependent Γ in our formalism) at low temperatures which overtake the timescale of experiments so ergodicity is lost. For spin ice the evidence

for this comes from the experiments of Refs. 28 and 29, which report a strong slowdown of the dynamics setting in around 1–2 K, a signature of which is the appearance of hysteresis in magnetization measurements. Consequently we need to examine whether the equilibrium computations of the this paper represent measurable quantities.

The good news is that the thermodynamic and static quantities are indeed still measurable. For the magnetization and the static structure factor this is a consequence of self-averaging in the sample—with probability one these quantities are the same for a configuration picked at random as they are for the entire ensemble of ground states. This in turn comes from two sources. First, even in a frozen three dimensional configuration, the different *kagome* planes effectively give different members of the equilibrium two dimensional ensemble. Second, even in a given plane we get self-averaging. For example, the spin-spin correlation function at a fixed separation, averaged over the location of the spins in a configuration picked at random, converges to its ensemble averaged value in the limit of infinite system size; the algebraic correlations in our problem lead to at best a $(\ln N)^{1/2}$ correction to the $1/\sqrt{N}$ dependence expected for the fluctuations in a system with N sites. As the structure factor involves exactly this average, all is well on that front. The same holds for the magnetization, measured as the moment frozen into a field cooled sample.

The story with the entropy is different. Indeed it is worth emphasizing the remarkable fact that experiments measure an entropy associated with a macroscopic degeneracy of ground states even as the system settles into just one of them (or a submacroscopic number since local fluctuations presumably do survive even as large scale rearrangements are frozen out). The contradiction with the statistical mechanical view of entropy as the logarithmic volume of phase space explored is resolved when one notes that the experimental determination consists of starting with the known entropy of the paramagnetic high temperature state and integrating down with the measured heat capacity. At issue then is whether the freezing substantially affects the ratio of heat capacity to temperature over the temperature range where it is significant. For the ice problems, the spectrum involves a finite gap to making a defect above the ground state manifold. Consequently, at temperatures below this gap, which is also where freezing takes place, the heat capacity is exponentially small in the temperature, whence the freezing hardly affects the entropy determination.[30] In our problem this implies that field cooled measurements of the heat capacity will allow determination of the thermodynamic entropy inclusive of tilted field values.

VI. THERMAL AND ANALYTIC DEFECTS

Thus far our analysis has assumed that the only accessible configurations belong to the ground state manifold of the pseudospin Hamiltonian. To make contact with experiments we need to examine the effects of relaxing this restriction. In this section we do this, thereby obtaining some insight into the low and high field boundaries of the plateau and also

comment on a couple of other salient limitations of our analysis.

As noted earlier, at $T=0$ simple energetics shows that the plateau extends over $0 < g\mu_B JB < 6J_{\text{eff}}$, giving way at zero field to the full spin ice ground state manifold and to the right to the fully saturated state. At finite temperatures the plateau state is no longer field independent but will instead evolve, especially near the transitions. At low temperatures we can gain insight into this evolution by examining the thermally excited defects that will dress the critical dimer state that we have discussed in this paper.

A. Monomer defects

The first defect to consider increases the local magnetization and it is the condensation of such defects which terminates the plateau at its high field end. The local minimum energy process to consider is one in which a down pseudospin in a *kagome* plane is converted to an up pseudospin so that all spins of the two triangles that share it are now aligned with the field. Such a process violates the ice rule as there are now two tetrahedra with $\Sigma_\kappa \sigma_\kappa \neq 0$, and takes us out of the ground state manifold. A single flipped spin in fact corresponds to a *pair* of defects, which is most easily seen in the dimer representation where it corresponds to two monomers on adjacent sites of the hexagonal lattice. The two partners of the pair can be separated by moving one of the defects, on an "up" triangle, say, to a neighboring up triangle. This is done by flipping two spins on an adjacent "down" triangle, namely, the $\sigma = -1$ spin and the spin it shares with the up triangle. This puts the original up triangle back into the spin ice ground state at the expense of violating the constraint on the up triangle sharing the spin with the down triangle. It follows then that the energy cost of flipping the spin is the creation energy $2\mathcal{E}_m = 4J_{\text{eff}} - 2g\mu_B JB/3$ of two defects. This energy vanishes exactly at critical field $g\mu_b JB_c = 6J_{\text{eff}}$ which separates the two plateaux at $T=0$.[5,10]

At finite but low temperatures, the system contains a finite but small density of these defects whose separation will set a correlation length and cutoff the critical singularities of the parent dimer state. Naively, we might anticipate $\xi^2 \sim 1/n_m \sim \exp(\mathcal{E}_m/k_B T)$ but there is a pseudo-Coulomb (logarithmic) entropic interaction between them that modifies this dependence. The exact dependence can be computed by an energy-entropy balance argument that is equivalent to a tree level renormalization group computation.[31] Consider a system of area A and let $Z(\mathbf{r_1}, \mathbf{r_2})$ be the number of configurations of the dimers (spin background) in the presence of the two monomers (defects) held fixed at positions $\mathbf{r_1}$ and $\mathbf{r_2}$ while Z is the number of configurations of the dimers with no monomers present. Then the free energy cost of introducing two defects is

$$\Delta F = 2\mathcal{E}_m - T \ln \int d^2 r_1 \int d^2 r_2 Z(\mathbf{r_1}, \mathbf{r_2})/Z. \quad (6.1)$$

The ratio $Z(\mathbf{r_1}, \mathbf{r_2})/Z$ can be computed by height representation theory by noting that monomers on the two sublattices correspond to a height mismatch of ± 3 when encircled. The operator identification described in Ref. 26 then implies

$$Z(\mathbf{r}_1,\mathbf{r}_2)/Z \sim 1/\sqrt{|\mathbf{r}_1-\mathbf{r}_2|}, \qquad (6.2)$$

which is the same decay first described in Ref. 32 for the closely related square lattice dimer problem. With this in hand, it is easy to see that $\Delta F < 0$ when the system size ξ, which we now identify with the correlation length is given by

$$\xi^2 \sim 1/n_m \sim \exp\!\left(\frac{8\mathcal{E}_m}{7k_BT}\right). \qquad (6.3)$$

B. Termination of the plateau by monomers

At a fixed location in the plateau the above formula will describe the asymptotic low-temperature approach to the purely dimer manifold. At a fixed temperature though this analysis will break down near B_c where a treatment of the statistical mechanics of large numbers of defects needs to be devised. We expect to address this problem in more detail elsewhere and here we will content ourselves with three remarks.

First, matters simplify in a scaling limit $T \to 0$ and $B \to B_c$ with $(B-B_c)/T$ fixed. In this limit we can ignore all spin configurations save those consisting of dimer configurations "doped" with some number of monomers. The remaining problem is the noninteracting monomer-dimer problem and hence the interpolation between the two plateaux as a function of B is a crossover and not a phase transition.[33] Second, at the transition field, this leads to an equal weight sum over all monomer-dimer configurations. The entropy at this point is then higher than it is in the low field plateau before it turns around and then heads for zero deep into the high field plateau. Third, the transition point exhibits a temperature independent ensemble in this treatment which should lead to a crossing point for the magnetization isotherms. Above a critical temperature, the data[16] indeed exhibit a maximum in the entropy and a crossing point for the magnetization isotherms. Below this temperature the crossover appears to turn into a first order transition at which point the entropy plummets with temperature and the magnetization develops a discontinuity.[16] *Prima facie* this appears to be a puzzle for the nearest-neighbor model considered in this paper, although it is possible that a purely mean field treatment of the longer ranged pieces of the dipole interaction omitted here renormalize B sufficiently to turn the sharp low-temperature crossover into a transition.

C. String defects

The second type of defect to consider is responsible for decreasing the magnetization towards the low field end of the plateau. As in this limit we must preserve the ice rule, decreasing the magnetization requires that we flip a spin on the triangular sublattice $\kappa=0$ while satisfying the ice rule by choosing a second spin in the *kagome* plane to have $\sigma=-1$. Interestingly, this is not enough since the $\kappa=0$ spin is shared by another tetrahedron and so on. Indeed, one can see quite generally that it must be infinite in length. This follows from the observation that the local ice rule leads to the global property that all [111] triangular planes have the

same magnetization, which is equal and opposite to that of all *kagome* [111] planes.[34] As the magnetization of the triangular [111] layers is saturated, reducing it by flipping one of its spins in one layer requires flipping one spin in all of the other layers at the same time. The energy of such a defect $\mathcal{E}_s$ is thence most conveniently quoted per (*kagome* and triangular bi-) layer. As it involves antialigning a spin in the triangular and one in the *kagome* layer with the field, we have $\mathcal{E}_s = 8g\mu_BJB/3$. Remarkably, despite the energy cost proportional to the linear system size L it is still entropically favored in a large system. To see this, note that such a defect corresponds to inserting a surplus dimer, violating the hard core condition, into each *kagome* plane, which connects a (say) up triangle above which a spin on sublattice $\kappa=0$ is flipped with a down triangle below which the next flipped $\kappa=0$ spin is located. As in the case of the pair of monomers defects, the pair of triangles can again be separated into two distinct defects—in dimer language into two sites with two dimers each. If the separation of these sites were to cost no (in plane) entropy, one would be free to choose which of the A spins in the triangular layer to flip, thereby endowing the defect with an entropy of $\mathcal{S}_2 = \ln A$ per layer. For a sufficiently large system, it would therefore always be free energetically favorable to generate such a defect.

The actual density of such defects is lowered by the same in-(*kagome*)plane entropic mechanism discussed for monomer defects. Again we appeal to height representation theory to find that sites with two dimers carry charge ± 3 so that the entropic interaction between them is the same as for two monomers. This implies that per layer the entropic gain from being able to pick the separation of the defects grows as $\ln\int^{\sqrt{A}} r^{-1/2}r\,dr \sim (3/4)\ln A$. From this we deduce that a cylinder of cross sectional area A first nucleates this string defect when $3/4\ln A = (8/3)g\mu_BJB$ whence we expect the area density and hence transverse correlation length set by

$$\xi^2 \sim 1/n_s \sim \exp[32g\mu_BJB/9k_BT] \qquad (6.4)$$

at low temperatures. This exponential dependence will then determine the approach of the magnetization to its plateau value at a fixed low field as temperature is lowered.

Again, the proliferation of such defects at low fields but fixed temperature requires a different treatment, involving a linear response calculation about the full spin ice manifold, which we will discuss elsewhere. In this regime all relevant energies are set by the field so that physical quantities will be functions of B/T alone. We expect then that the magnetization curves will collapse with a finite slope at the origin when plotted as a function of B/T.

We can draw one further inference from our computation of the defect densities. By equating the activation energies of the two defects we can identify the field at which their densities cross at the lowest temperatures—this will also be the field at which the magnetization isotherm crosses the zero field value of the magnetization at low temperatures and hence a second crossing point. This yields a field $g\mu_BJB = (18/31)J_{\text{eff}}$ which is about a tenth of the critical field between the plateaus.

How does the presence of such defects alter the results we have described above? Fundamentally, their presence will of course make itself known as a deviation from the "exact" result; in particular, the smallest of the defect induced finite correlation lengths will determine the cutoff at which, for example, the logarithmic peaks in the neutron scattering stop growing.

As for the Kasteleyn transition, both types of defects will inevitably smear out the fluctuation-free regime and therefore the mixed first/second order nature of the transition. Monomer defects can be exponentially suppressed by lowering the temperature (compared to J). As one lowers the temperature at small fields $B/T \ll 1$, the angle $\sin \phi$ at which the transition takes place decreases inversely with B/T, whereas the density of string defects is exponentially suppressed. By achieving an improved angular resolution, the crossover from Kasteleyn behavior to a more conventional second order phase transition could thus be reduced.

D. Disorder and dipoles

Finally we turn to two significant limitations of our analysis in this paper. First, actual samples are likely to contain structural defects due simply to chemical disorder such as vacancies or interstitials affecting site occupancy or exchange paths. We are not aware of a determination of the density of such defects, although for Heisenberg spins on the related SCGO lattice, there have been both experimental[35,36] and theoretical[37] attempts to determine the density of vacancies from thermodynamic[35,37] or NMR experiments.[36] As the chemical defect density in single crystals tends to be higher than in powder samples, this might be a not insubstantial effect in this context.

The second important feature omitted from the nearest-neighbor spin ice model are the effects of the long-range dipolar interactions beyond the nearest-neighbor piece, which are sizeable due to the large spin of the dysprosium ion. We have already alluded to one possible effect in our discussion of the transition between the two plateaux, namely, that the polarization of the spins may require a self-consistent treatment of the field B that acts upon them. While this is always necessary when a macroscopic magnetization is present, in our case the issue is somewhat more delicate since the largest piece of the dipolar interactions has already been accounted for in the nearest-neighbor model.

On a fundamental level, however, the long-range dipolar interactions do not seem to lead to a significant interplane ordering effect, as this would have reduced the entropy determined in the experiment. This may, however, be a consequence not of the precise thermodynamic behavior of the spin ice Hamiltonian in a field, but rather an indication of the magnet's inability to access its true ground state in the presence of energy barriers as discussed in Section II.

VII. SUMMARY

The application of a field in the [111] direction to the spin ice compounds leads, by a reasonable set of approximations,

to an elegant dimensional reduction of the three-dimensional problem onto a set of decoupled two-dimensional problems. Fortunately, the resulting two-dimensional problem is one of planar dimers and hence is exactly soluble, so that the statics and thermodynamics can be determined exactly.

In particular, we have determined the entropy of the magnetization plateau, and calculated the spin correlations in this regime. These lead to the neutron scattering cross sections depicted in Figs. 5,6, which display peaks the height of which in principle grows logarithmically with system size. However, their growth is cut off by different types of defects inducing a finite correlation length, as discussed in Sec. VI.

Upon tilting the field, we have shown that these peaks move towards the zone center. They reach the zone center at the Kasteleyn transition, which has a mixed first/second order character, exhibits anisotropic scaling, and displays a divergence of the specific heat. From an analysis of the dynamical properties of the plateau regime, we predict dynamical scaling with an exponent $z_d = 2$, and discuss the expected shape and scaling of peaks measured in inelastic neutron scattering.

While the computed entropy has already been measured, the predictions for the correlations can be tested by scattering. Also testable are thermodynamic and static predictions for a Kasteleyn transition upon tilting the field in the [-1-12] direction and for the dynamic correlation in the plateau. Finally we have sketched a theory of the finite temperature modifications which we intend to flesh out in future work.[38]

From the viewpoint of spin ice physics, it is fortunate that much existing technology turns out to be especially suited to this task. From the perspective of statistical mechanics the realization of the hexagonal dimer model as well as of the monomer-dimer problem in a three-dimensional system with built in self-averaging and easy access via neutron scattering, in contrast to surface or interface realizations, is surely interesting.

Sadly it does not appear possible to make one final link—to the *quantum* dimer model on the hexagonal lattice[39–41] as this would require a "resonance" quantum dynamics consisting of a simultaneous coherent tunneling of six pseudospins which is rather unlikely given the large spin $J = 15/2$ of the constituents. We leave the realization of this physics as a challenge for future work.

ACKNOWLEDGMENTS

[1] M.J. Harris, S.T. Bramwell, D.F. McMorrow, T. Zeiske, and K.W. Godfrey, Phys. Rev. Lett. **79**, 2554 (1997).

[2] A.P. Ramirez, A. Hayashi, R.J. Cava, R. Siddharthan, and B.S. Shastry, Nature (London) **399**, 333 (1999).

[3] P.W. Anderson, Phys. Rev. **102**, 1008 (1956).

[4] S.T. Bramwell and M.J. Harris, J. Phys.: Condens. Matter **10**, L215 (1998).

[5] R. Siddharthan, B.S. Shastry, A.P. Ramirez, A. Hayashi, R.J. Cava, and S. Rosenkranz, Phys. Rev. Lett. **83**, 1854 (1999); R. Siddharthan, B.S. Shastry, and A.P. Ramirez, Phys. Rev. B **63**, 184412 (2001).

[6] B.C. den Hertog and M.J.P. Gingras, Phys. Rev. Lett. **84**, 3430 (2000); R.G. Melko, B.C. den Hertog, and M.J.P. Gingras, *ibid.* **87**, 067203 (2001).

[7] S.T. Bramwell and M.J.P. Gingras, Science **294**, 1495 (2001).

[8] J. T. Chalker and P. Chandra (private communication).

[9] R. Moessner, Phys. Rev. B **57**, R5587 (1998).

[10] M.J. Harris, S.T. Bramwell, P.C.W. Holdsworth, and J.D.M. Champion, Phys. Rev. Lett. **81**, 4496 (1998).

[11] S.T. Bramwell, M.J. Harris, B.C. den Hertog, M.J.P. Gingras, J.S. Gardner, D.F. McMorrow, A.R. Wildes, A.L. Cornelius, J.D.M. Champion, R.G. Melko, and T. Fennell, Phys. Rev. Lett. **87**, 047205 (2001).

[12] T. Fennell, O.A. Petrenko, G. Balakrishnan, S.T. Bramwell, J.D.M. Champion, B. Fak, M.J. Harris, and D. McK. Paul, cond-mat/0107414 (unpublished).

[13] A.L. Cornelius and J.S. Gardner, Phys. Rev. B **64**, 060406 (2001).

[14] O.A. Petrenko, M.R. Lees, and G. Balakrishnan, cond-mat/0211282 (unpublished).

[15] K. Matsuhira, Z. Hiroi, T. Tayama, S. Takagi, and T. Sakakibara, J. Phys.: Condens. Matter **14**, L559 (2002).

[16] Z. Hiroi, K. Matsuhira, S. Takagi, T. Tayama, and T. Sakakibara, J. Phys. Soc. Jpn. **72**, 411 (2003).

[17] R. Moessner and S.L. Sondhi, Phys. Rev. B **63**, 224401 (2001).

[18] The mapping of a *kagome* Ising magnet in a field onto a hexagonal lattice quantum dimer model has been rediscovered by M. Udagawa, M. Ogata, and Z. Hiroi, J. Phys. Soc. Jpn. **71**, 2365 (2002).

[19] C.S.O. Yokoi, J.F. Nagle, and S.R. Salinas, J. Stat. Phys. **44**, 729 (1986).

[20] P.W. Kasteleyn, Physica (Amsterdam) **27**, 1209 (1961); J. Math. Phys. **4**, 287 (1963).

[21] C.L. Henley, J. Stat. Phys. **89**, 483 (1997).

[22] A different possibility is the selection of a unique state in the ice manifold by quantum effects, e.g., as discussed for two-dimensional ice by R. Moessner, Oleg Tchernyshyov, and S.L. Sondhi (cond-mat/0106286),[42] but that prospect is also irrelevant to observations under laboratory conditions.

[23] This is distinct from the *kagome* spin ice model studied by A.S. Wills, R. Ballou, and C. Lacroix, Phys. Rev. B **66**, 144407 (2002), where an easy axis ferromagnet on the *kagome* lattice is studied. This model maps onto a *kagome* Ising magnet in zero field, which in turn relates to our model only under a rather unnatural choice of field.

[24] B.S. Shastry, cond-mat/0210230 (unpublished).

[25] This expression differs by an overall sign from Eq. (37) of Ref. 19. It combines (in their notation) C_{vv} and $C_{vv'}$, allowing for half integer values of x. The oscillation period, for a fixed angle θ' of this expression varies as $1/\cos\theta'$, as noted in Ref. 19. This is a consequence of the projection of the period of oscillation in the x direction onto the direction determined by θ'.

[26] H.W.J. Blöte and H.J. Hilhorst, J. Phys. A **15**, L631 (1982); B. Nienhuis, H.J. Hilhorst, and H.W. Blöte, *ibid.* **17**, 3559 (1984).

[27] C. Zeng and C.L. Henley, Phys. Rev. B **55**, 14 935 (1997).

[28] J. Snyder, J.S. Slusky, R.J. Cava, and P. Schiffer, Nature (London) **413**, 48 (2001); J. Snyder, B.G. Ueland, J.S. Slusky, H. Karunadasa, R.J. Cava, A. Mizel, and P. Schiffer, cond-mat/0302453 (unpublished).

[29] K. Matsuhira, Y. Hinatsu, and T. Sakakibara, J. Phys.: Condens. Matter **13**, L737 (2001).

[30] Thus the equality of the measured entropy and its equilibrium computation is not a consequence of self-averaging. Indeed the temperature range where the system freezes and we need to invoke self-averaging contributes nothing to the entropy determination since it is characterized by a zero heat capacity (a temperature-independent internal energy).

[31] J. L. Cardy, *Scaling and Renormalization in Statistical Physics* (Cambridge University Press, Cambridge, 1996).

[32] M.E. Fisher and J. Stephenson, Phys. Rev. **132**, 1411 (1963).

[33] O.J. Heilmann and E.H. Lieb, Phys. Rev. **24**, 1412 (1970).

[34] R. Moessner and J.T. Chalker, Phys. Rev. Lett. **80**, 2929 (1998); Phys. Rev. B **58**, 12 049 (1998).

[35] P. Schiffer and I. Daruka, Phys. Rev. B **56**, 13 712 (1997).

[36] L. Limot, P. Mendels, G. Collin, C. Mondelli, B. Ouladdiaf, H. Mutka, N. Blanchard, and M. Mekata, Phys. Rev. B **65**, 144447 (2002).

[37] R. Moessner and A.J. Berlinsky, Phys. Rev. Lett. **83**, 3293 (1999); C.L. Henley, Can. J. Phys. **79**, 1307 (2001).

[38] R. Moessner and S. L. Sondhi (unpublished).

[39] D.S. Rokhsar and S.A. Kivelson, Phys. Rev. Lett. **61**, 2376 (1998).

[40] N. Read and S. Sachdev, Phys. Rev. B **42**, 4568 (1990).

[41] R. Moessner, S.L. Sondhi, and P. Chandra, Phys. Rev. Lett. **84**, 4457 (2000); Phys. Rev. B **64**, 144416 (2001).

[42] R. Moessner, Oleg Tchernyshyov, and S.L. Sondhi, cond-mat/0106286 (unpublished).